HHS Public Access

Author manuscript

Adv Funct Mater. Author manuscript; available in PMC 2024 January 03.

Published in final edited form as:

Adv Funct Mater. 2023 January 03; 33(1): . doi:10.1002/adfm.202206936.

Nanofiber Aerogels with Precision Macrochannels and LL-37-Mimic Peptides Synergistically Promote Diabetic Wound Healing

Johnson V. John[§],
Department of Surgery-Transplant and Mary & Dick Holland Regenerative Medicine Program, College of Medicine, University of Nebraska Medical Center, Omaha, Nebraska 68198, United States

Terasaki Institute for Biomedical Innovation, Los Angeles, CA, 90064, United States

Navatha Shree Sharma[§],
Department of Surgery-Transplant and Mary & Dick Holland Regenerative Medicine Program, College of Medicine, University of Nebraska Medical Center, Omaha, Nebraska 68198, United States

Guosheng Tang,
Division of Engineering in Medicine, Department of Medicine, Brigham and Women's Hospital, Harvard Medical School, Cambridge, MA 02139, United States

Zeyu Luo,
Division of Engineering in Medicine, Department of Medicine, Brigham and Women's Hospital, Harvard Medical School, Cambridge, MA 02139, United States

Yajuan Su,
Department of Surgery-Transplant and Mary & Dick Holland Regenerative Medicine Program, College of Medicine, University of Nebraska Medical Center, Omaha, Nebraska 68198, United States

Shelbie Weihs,
Department of Surgery-Transplant and Mary & Dick Holland Regenerative Medicine Program, College of Medicine, University of Nebraska Medical Center, Omaha, Nebraska 68198, United States

S. M. Shatil Shahriar,
Department of Surgery-Transplant and Mary & Dick Holland Regenerative Medicine Program, College of Medicine, University of Nebraska Medical Center, Omaha, Nebraska 68198, United States

Guangshun Wang,
Department of Pathology and Microbiology, College of Medicine, University of Nebraska Medical Center, University of Nebraska Medical Center, Omaha, Nebraska 68198, United States

[*] jingwei.xie@unmc.edu .
[§]These two authors contributed equally to this work

Conflic of Interest
The authors declare no conflict of interest.

Alec McCarthy,
Department of Surgery-Transplant and Mary & Dick Holland Regenerative Medicine Program, College of Medicine, University of Nebraska Medical Center, Omaha, Nebraska 68198, United States

Justin Dyke,
Department of Surgery-Transplant and Mary & Dick Holland Regenerative Medicine Program, College of Medicine, University of Nebraska Medical Center, Omaha, Nebraska 68198, United States

Yu Shrike Zhang,
Division of Engineering in Medicine, Department of Medicine, Brigham and Women's Hospital, Harvard Medical School, Cambridge, MA 02139, United States

Ali Khademhosseini,
Terasaki Institute for Biomedical Innovation, Los Angeles, CA, 90064, United States

Jingwei Xie*
Department of Surgery-Transplant and Mary & Dick Holland Regenerative Medicine Program, College of Medicine, University of Nebraska Medical Center, Omaha, Nebraska 68198, United States

Department of Mechanical and Materials Engineering, College of Engineering, University of Nebraska Lincoln, Lincoln, NE 68588, United States

Abstract

Fast healing of diabetic wounds remains a major clinical challenge. Herein, this work reports a strategy to combine nanofiber aerogels containing precision macrochannels and the LL-37-mimic peptide W379 for rapid diabetic wound healing. Nanofiber aerogels consisting of poly(glycolide-*co*-lactide) (PGLA 90:10)/gelatin and poly-*p*-dioxanone (PDO)/gelatin short electrospun fiber segments were prepared by partially anisotropic freeze-drying, crosslinking, and sacrificial templating with three-dimensional (3D)-printed meshes, exhibiting nanofibrous architecture and precision micro-/macrochannels. Like human cathelicidin LL-37, W379 peptide at a concentration of 3 μg/mL enhanced the migration and proliferation of keratinocytes and dermal fibroblasts in a cell scratch assay and a proliferation assay. *In vivo* studies show that nanofiber aerogels with precision macrochannels can greatly promote cell penetration compared to aerogels without macrochannels. Relative to control and aerogels with and without macrochannels, adding W379 peptides to aerogels with precision macrochannels shows the best efficacy in healing diabetic wounds in mice in terms of cell infiltration, neovascularization, and re-epithelialization. The fast re-epithelization could be due to upregulation of phospho-extracellular signal-regulated kinase (p38 MAPK) after treatment with W379. Together, the approach developed in this work could be promising for the treatment of diabetic wounds and other chronic wounds.

Graphical Abstract

A strategy was reported by combining nanofiber aerogels containing precision macrochannels and database-designed peptide W379 for rapid diabetic wound healing. The addition of the W379 peptide to aerogels with precision macrochannels leads to best efficacy in healing diabetic wounds

in mice in terms of cell infiltration, neovascularization, and re-epithelialization compared to other groups.

Keywords

Nanofiber aerogel; precision macrochannels; antimicrobial peptide W379; cell migration; diabetic wound healing

1. Introduction

Diabetes mellitus affects 23.6 million people in the United States and approximately 20–25% of diabetic patients will develop foot ulcers during the disease. [1–3] The direct annual expenditure toward managing these ulcers is $9 billion to $13 billion in the United States alone. [4–6] Diabetic foot ulcers (DFUs) are complex problems in diabetic Mellitus patients. Amputation is required in a significant number of DFUs patients each year, degrading the quality of their lives, increasing the societal burden, and reducing their life expectancy.[7,8] There is an urgent need for developing novel approaches to rapidly heal diabetic wounds.

Due to the similar architecture to the extracellular matrix, electrospun nanofibers have been widely examined in many biomedical applications, including wound healing, tissue engineering, and regenerative medicine.[9–12] Generally, nanofibers form two-dimensional (2D) membranes with limited thickness and small pore sizes, limiting their chances in various applications in tissue engineering.[13,14] Recently, an innovative gas-foaming method has been developed to transform 2D nanofiber membranes into three-dimensional (3D) objects with various shapes and controlled alignment; however, this method may limit the expansion of nanofiber mats with specific compositions (e.g., soft polymeric materials). [15–21] Apart from that, researchers have also developed different approaches to prepare 3D nanofiber aerogels with predesigned shapes based on short nanofiber segments using molding, freeze-drying, and crosslinking.[22–25] The aerogels consisting of short fiber segments can be made of any material (e.g., inorganic) that is capable of being processed into nanofibers by electrospinning. Although the nanofiber aerogels are porous, the small pore size and poor pore interconnectivity often lead to insufficient cell penetration, which constrains their applications in wound healing and tissue regeneration.[26] To address this issue, our recent study reported an aerogel with patterned macrochannels and microchannels using a sacrificial templating method. The subcutaneous study showed an enhanced cellular infiltration compared to the aerogels without templating.[26]

LL-37, the only member of the human cathelicidin family of antimicrobial peptides, exhibits many biological functions, including antimicrobial property, enhancement of the proliferation and migration of skin cells, promotion of vascularization and chronic wound healing, and regulation of inflammation.[27–30] However, several shortcomings are associated with native LL-37, such as instability to proteases (loss of activity) and high cost due to long sequence. To circumvent these drawbacks, much effort has been devoted to engineering LL-37-derived peptides. Recently, W379 (also dubbed verine) has been designed based on the antimicrobial peptide database (https://aps.unmc.edu). Compared to LL-37 (37 residues), W379 comprises only eight amino acids (sequence: RRRWWWWV).

The four tryptophans and arginines of W379 can be regarded as a close mimic of the key membrane-targeting amino acids (F5, F6, F17, F27, and arginines) of LL-37. Indeed, W379 maintains a broad-spectrum antimicrobial activity and simultaneously exhibits superiority in several aspects, including a unique amphipathic structure and a significant reduction in production cost.[31–34]

We showed the antibacterial efficacy of W379 in our previous studies, which can effectively remove biofilms from the artificial wounds created in human skin explants and type II diabetic mouse wounds without debridement.[35] Interestingly, LL-37 peptides exhibit many additional useful features other than antibacterial properties.[36–38] For example, LL-37 peptides stimulate angiogenesis by activating the formyl peptide receptor-like 1 receptor.[36] Usually, hCAP18/LL-37 expression is increased in the injured skin, while hCAP18/LL-37 level is low in the skin with developed chronic ulcers.[39] LL-37 peptide transactivation of the epidermal growth factor receptor (EGFR) stimulates keratinocyte migration during wound healing.[37] In contrast, anti-LL-37 Ab prevents the re-epithelialization of wounds on the skin.[39] It has been reported that SOCS3/CIS3 inhibits STAT3 phosphorylation and hepatocyte growth factor-induced migration of human keratinocytes.[38] Keratinocyte migration induced by LL-37 peptide may be mediated through the STAT3-SOCS/CIS family.[38] These findings demonstrated that LL-37 plays a crucial role in the wound healing process.

Inspired by the multiple functions of LL-37 peptides, we aim to investigate the effect of LL-37 mimicking W379 peptides on cell migration and reepithelization in a type II diabetic mouse wound healing model. Besides that, innovative wound dressing materials that contain patterned macrochannels can facilitate nutrient and oxygen supply to accelerate wound healing, to avoid scar formation in a chronic wound. Therefore, the main objective of this study is to examine the synergistic influence of molecularly engineered W379 peptides composed of aerogel with precision micro/microchannel for rapid diabetic wound healing. The micro/macro channel containing nanofiber aerogels are composed of poly(glycolide-*co*-lactide) (PGLA 90:10)/gelatin and poly-p-dioxanone (PDO)/gelatin short nanofibers as these raw materials have been used in the United States Food and Drug Administration (FDA)-approved wound care products (e.g., sutures, dressings, hemostatic materials).[40–42] Such aerogels could be used for promoting diabetic wound healing after debridement. The synergistic influence of patterned macrochannels and W379 in nanofiber aerogels can boost vascularized granulation tissue production and re-epithelialization in diabetic wound healing. Here, we examine the effects of W379 and patterned macrochannels in aerogel dressings on skin cell proliferation, migration, neovascularization, and reepithelization.

2. Results and Discussion

Sacrificial template-based macro/micro channel engineering in the biomaterial has become much attention in tissue engineering due to its better nutrient and oxygen supply and guided cell migration.[26] Among them, our PCL/gelatin nanofiber short nanofiber aerogels with patterned macro/micro channels showed rapid cell migration in *in vitro* studies as well as in subcutaneous rat models.[26] Unfortunately, the PCL-composed aerogel degradation rate is slow.[43] To overcome these issues here, we aimed to engineer rapidly degradable nanofiber

aerogels with precision macrochannels made of PGLA/gelatin(1:1) and PDO/gelatin(1:1) (faster degradable polymers) short nanofibers. Then we combined LL 37-mimetic W379 peptides with aerogels for examining the synergistic influence of both aerogel and W379 peptides in diabetic wound healing.

Figure 1 shows the schematic representation of the fabrication of nanofiber aerogels with precision macrochannels. We first generated PGLA/gelatin (1:1) and PDO/gelatin (1:1) nanofibers via electrospinning (Figure S1). The average diameter of the PDO:gelatin and PGLA:gelatin nanofibers was 600 ± 200 nm. Then, nanofibers were chopped into short nanofibers with 20 to 50 μm lengths by cryocutting following our previously established protocols with slight modifications.[24–26] Then, the PGLA/gelatin:PDO/gelatin (1:1) (25 mg/mL) short nanofibers in water with 5% gelatin relative to the fiber content were homogenized using ultrasonication. The addition of gelatin can enhance the stability of the dispersion during homogenization. A predetermined volume of the short nanofiber suspension was added to a copper (Cu) mold that contained 3D-printed alginate meshes as a sacrificial template. The nanofiber suspension in the mold was then quickly frozen using a partially anisotropic freezing configuration.[26] The formation of sacrificially templated aerogels was achieved by lyophilizing frozen short nanofiber suspensions. To improve mechanical properties, the freeze-dried samples were removed from the molds and crosslinked with glutaraldehyde (GA) vapor overnight using Schiff-base chemistry. The sacrificial alginate templates were then removed by immersing the aerogels in a 50-mM ethylenediaminetetraacetic acid (EDTA) solution for 4–6 h. The aerogels were sterilized with 70% ethanol prior to in vitro and in vivo experiments. The same procedure was used to create nanofiber aerogels without templated macrochannels, except that no sacrificial templates were used during the freeze-casting process.

Figure 2 shows SEM images of nanofiber aerogels consisting of PGLA/gelatin:PDO/gelatin short nanofibers without and with precision macrochannels. Figure 2A shows the morphology of cross-sections of nanofiber aerogels without sacrificial templating, displaying a porous and ordered lamellar structure, while Figure 2B shows the vertical and horizontal cross-section images of nanofiber aerogels with sacrificial templating, exhibiting patterned macrochannels and an aligned lamellar structure between the macrochannels, which are in line with our previous observations.[26] Moreover, the diameters of macrochannels were approximately 300–500 μm, which could be optimal for cell migration and nutrient supply from the tissue engineering perspective. Interestingly, both aerogels maintained the extracellular mimetic nanofibrous architecture.

Inspired by the multiple functions of LL-37 peptides, here we attempted to assess the efficacy of W379 peptide on cell migration and reepithelization. In particular, we performed cell viability assay to explore the potential cytotoxicity of the LL-37-mimetic peptide W379 in two types of skin cells including human keratinocytes (HaCat cell line) and primary human dermal fibroblasts (HDF). Figure S2 shows HaCat and HDF cell viability under different concentrations of W379 peptides ranging from 1 μg/mL to 7 μg/mL. Figure S2A shows the viability of HaCat cells after 24-h treatment with W379, indicating that ~98% of cells were viable after treatment with 1 μg/mL of W379 peptide, and ~93% of cells were viable after treatment with 3 μg/mL of W379 peptide, but the viability decreased to

75% and 80% after treatment with W379 peptide at higher concentrations such as 5 and 7 μg/mL, as compared with nontreated cells. In contrast, we found a different trend for W379 peptide-treated HDF at concentrations ranging from 1 μg/mL to 7 μg/mL. Figure S2B shows the viability of W379 peptide-treated HDF cells. It is seen that HDF showed almost ~100% cell viability after treatment of W379 peptide at concentrations from 1 μg/mL to 5 μg/mL as compared with the control (non-treated cells). However, at 7 μg/mL, the W379 peptide showed some cytotoxicity, and only 75% of cells were viable after 24-h treatments.

After confirming the cell viability of the W379 peptide we analyzed the cell migration capacity of short peptide W379 and compared it with the long LL37 peptide via an established artificial wound (scratch assay) using HaCat and HDF cell monolayers. Figure 3, A-D, shows the HaCat and HDF scratch assay images after treatment with W379 and LL-37 peptides at different concentrations (0–7 μg/mL) for 12 h and 24 h. Figure S3 and Figure S4 show the high quality images of Figure 3A–D for better visualization of the difference in cell migration. The results show that the W379 peptide and LL-37 peptide can significantly enhance both cell migration in scratch assay when compared to the control. The W379 peptide-treated cells showed a similar migration as LL-37 peptide-treated cells. We quantified W379 and LL-37 peptides-induced cell migration in the scratched area using Image J (Figure 3, E and F). After incubation for 12 h and 24 h, the migrated cells (HaCat and HDF) were analyzed in the artificial wound (scratched area). Figure 3E shows that the migrated HaCat cells covered almost ~90% of the wound area after treatment with 3 μg/mL of LL-37 peptide. However, the cell surface coverage decreased to ~75% at higher concentrations (e.g., 5 μg/mL and 7 μg/mL). In contrast, the cell migration capacity increased with increasing the concentrations of W379 peptide. In addition, we did not observe any significant difference in cell migration between W379 and LL37 treated HDF wounds at concentrations ranging from 3 to 7 μg/mL (Figure 3F).

To evaluate the synergistic healing efficacy of nanofiber aerogels with and without macro/micro channels and LL-37 mimetic W379 peptide *in vivo*, we created an 8-mm full-thickness skin wound model using type 2 diabetic mice to examine their healing efficacy. Initially, we noted that mice had blood glucose levels ranging from 310 mg/dl to 496 mg/dl, significantly higher than the usual 200 mg/dl. In addition, the body weight of the mice ranged from 36.5 g to 44.8 g. There was no statistically significant difference in body weight between the mice before and after the procedure. We investigated wound healing after treatment for 7 and 14 days. Figure S5A shows the photographs of the wounds before and after implantation of nanofiber aerogels on day 0. To avoid wound contraction we tethered the splint around the wound to maintain the wound shape and expected a uniform cell migration from the side to the center of the aerogels. Figure S5B shows the photographs of the wounds treated with aerogels without macrochannels (Aerogel-NC), aerogels with precision macrochannels (Aerogel-WC), aerogels with precision macrochannels and W379 peptides (Aerogel-WC+W379), and control with no treatment. As anticipated, no contraction was noticed due to the splint attachment.

Figure 4 shows the H & E staining images of diabetic wounds after treatment for 7 and 14 days. We could not observe cell infiltration into the wounds in the control group that received no therapy. In the case of the Aerogel-NC group, cell migration around the

aerogels was observed, which is similar to our previous subcutaneous investigation.[26] The Aerogel-WC and Aerogel-WC+W379 groups show greater cellular infiltration throughout the aerogels because the sacrificial template-induced macrochannels in the aerogels can provide routes for cell migration/infiltration throughout the aerogels. During the first week of treatment, we did not observe any significant cellular infiltration in both Aerogel-WC and Aerogel-WC+W379 groups. But, after two weeks, the migrated cells occupied ~70% of the regions of the aerogels (Aerogel-WC and Aerogel-WC+W379). It seems that the templated macrochannels played an important role in the granulation tissue formation (indicated by red arrows) in both Aerogel-WC and Aerogel-WC+W379 groups as compared with the control and Aerogel-NC groups (Figure 4). Figure S6 shows Masson's trichrome staining of harvested wounds and surrounding tissues, revealing that the wounds treated with Aerogel-NC, Aerogel-WC, Aerogel-WC+W379 had greater collagen deposition and new tissue formation than the wounds treated by the control group on both days 7 and 14. Furthermore, it appears that more blood vessels formed in wounds treated by the Aerogel-WC and Aerogel-WC+W379 groups when compared to the control and Aerogel-NC groups on day 14.

Based on the cell migration, we quantified the area of cell infiltration and neovascularization of the treated diabetic wounds. Figure 5 shows the quantification of cellular infiltration and neovascularization in the wounds after treatment for 7 and 14 days. While compared with the control and Aerogel-NC groups, the cells migrated into ~20% of the areas of the wound in 7 days, and further migrated throughout the aerogels and reached ~70% of the areas of the wounds within 14 days for the Aerogel-WC and Aerogel-WC+W379 groups (Figure 5A). We did not observe a significant difference in the cell migrated area of the wounds between the Aerogel-WC group and the Aerogel-WC+W379 group after 7 days of implantation, while there was a significant difference in the cell migrated area of the wounds between these two groups after implantation for 14 days. Intriguingly, the number of newly regenerated blood vessels inside wounds in the Aerogel-WC and Aerogel-WC+W379 groups was considerably higher than the number of newly formed blood vessels inside wounds in the control Aerogel-NCs groups (Figure 5B). In addition, a higher number of blood vessels were seen in the Aerogel-WC+W379 group than in the Aerogel-WC group on day 14. To further examine the reepithelialization, we also performed immunohistochemical staining of cytokeratin 6a. Figure S7 shows cytokeratin 6a stained wound samples. The cytokeratin 6a immunostaining shows the keratinocyte layer (in brown color) on the top of the aerogels. Based on these images, the length of the re-epithelialized layer on the top of the aerogel was used to quantify the reepithelization (Figure S8). For the wounds treated by Aerogel-WC, reepithelialization initiated from the peripheral site of defects on day 7, but reepithelialization tongues failed to bridge the defects on day 14. While calculating the ratio of reepithelization, we observed that only 70% of reepithelialization was achieved on day 14. In contrast, Aerogel-WC+W379 treated wounds showed almost complete reepithelization (brown band) on day 14. While compared with the control and Aerogel-NC groups (< 20% of reepithelization ratio on day 14), aerogel-WC and Aerogel-WC+W379 groups seem to show better performance in terms of percentages of reepithelialization on day 14. Therefore, incorporating the W379 peptide into the nanofiber aerogels with precision channels could significantly enhance neovascularization and reepithelialization.

We further attempted to understand the mechanism of W379 peptide on wound healing. Since W379 peptide promoted the migration of HaCat cells, we examined the p38 MAPK and STAT3 signaling pathways involved in cell migration.[44,45] Protein analysis of HaCat cells incubated with W379 peptide showed a time-dependent up-regulation in the expression of phospho-p38 MAPK (Figure 6A). Compared to control (no treatment), the phospho-p38 MAPK expression in cells treated with W379 peptide showed a gradual increase from 0 to 3 h and dropped at 6 h. For comparison, no significant change was observed in the expression of phospho-p38 MAPK in cells treated with LL-37 peptide compared to the control (Figure 6A and 6C). The total p38 MAPK levels in W379 and LL-37 peptide-treated cells remained the same (Figure 6A and 6C). We further analyzed the status of phospho-STAT3 in all the three groups (Figure 6B and 6C). Our findings showed no significant change in the status of STAT3 phosphorylation. These data cumulatively indicate that the W379 peptide may specifically work through the p38 MAPK signaling pathway to promote cell migration.

One of the most common complications in diabetic patients is non-healing chronic wounds.[46] Traditional exudate dressings rely on homogeneous hydrophilic materials like hydrogels to absorb and retain exudate.[47] Unfortunately, pores in hydrogels remain closed due to the high absorption, which blocks cell migration and delays wound closure. Recently, we introduced new forms of ECM mimetic 3D nanofiber materials for guiding cell migration for tissue repair and regeneration.[13, 15–21, 24–26] Among them, 3D-printed meshes templated nanofiber aerogels with patterned micro-/macrochannels demonstrated the rapid cell migration/infiltration after subcutaneous implantation in rats.[26] Moreover, the presented fabrication method offers versatility and allows numerous biopolymers and synthetic polymers to be engineered into nanofiber aerogels with precision macrochannels. In this study, we engineered PGLA/gelatin: PDO/gelatin nanofiber aerogels for diabetic wound healing as these raw materials are used in FDA-approved wound care products (e.g., Vilet®, RESTRATA®, PDM®, Basik®, Gelfoam®). The macrochannels can be precisely engineered through the predesigned 3D-printed meshes in terms of diameter and architecture. The lamellar structures and interconnected macrochannels could be ideal for nutrient and waste transport and cell infiltration.

Human cathelicidin peptide LL-37 shows multiple biological functions including antibacterial properties and promotion of angiogenesis and cell migration. [27–30] However, this native peptide is associated with shortcomings such as long sequence (high cost) and instability. Therefore, minimal clinical translation has arisen due to high manufacturing costs and decreased performance than endogenous LL-37. To avoid these problems, Wang *et al.* recently reported a series of AMPs, including LL-37 engineered peptides and database-designed horine and verine.[32–34] Among them, W379 shows great promise in killing multi-drug-resistant Gram-positive and Gram-negative bacteria. However, other biological functions of the W379 peptide are unknown. In this study, we evaluated the ability of the W379 peptide in cell migration and diabetic wound healing in combination with nanofiber aerogels with precision macrochannels.

It was found that 1 to 3 μg/mL of W379 peptide can approximately increase the viability of skin cells up to 95%. Similar to LL-37 peptides, W379 peptides at concentrations ranging from 1 to 7 μg/mL can significantly promote wound closure in the *in vitro* scratch assay. For

example, LL-37 peptide-treated HaCat cells showed 70 to 90% (3 to 7 μg/mL) of the wound area closed within 24 h. Similarly, the W379 peptide-treated HaCat cells migrated much faster initially, and the migration efficiency of cells treated by the W379 peptide was able to match the cells treated by the LL-37 peptide. We also performed the cell migration study using the HDF. When compared with HaCat cells, HDF wound assay showed almost 100% wound closure after 24-h treatment with both LL-37 and W379 peptides at concentrations from 3 to 7 μg/mL.

We further evaluated the synergistic effect of nanofiber aerogels with and without precision macrochannels and W379 peptides on healing diabetic wounds in mice. The H&E and trichrome staining results clearly showed that the aerogels with precision macrochannels greatly enhanced the cell migration as compared with control and aerogels without macrochannels. Moreover, the incorporation of the W379 peptide significantly promoted neovascularization and reepithelization on diabetic wounds. Western blotting was used to explore the potential mechanism of W379 peptide in wound healing. Due to the enhanced HaCat cell migration by the W379 peptide, the p38 MAPK and STAT3 signaling pathways were examined. [44,45] After treatment with the W379 peptide, protein quantitation showed that the phospho-p38 MAPK expression level increased until 3 h and then dropped at 6 h. The phospho-p38 MAPK expression reached its maximum level after 6 h. In contrast, cells treated with LL-37 did not show maximum phospho- p38 MAPK expression level after 2 h and then began to decline. When cells were treated with either W379 or LL-37 peptide, the overall p38 MAPK levels were comparable. In addition, W379 peptide seemed to have no influence on the phosphorylation of STAT3. This arises a question as to why W379 can activate p38 MAPK signaling at lower concentration (3 μg/mL) than LL-37. One plausible explanation is that W379 which is amphipathic in nature has a shorter peptide sequence (8 amino acid residues) compared to LL-37. This shorter configuration could enable W379 to promote signaling more efficiently at low concentrations when compared to LL-37. Activation of the p38 MAPK signaling pathway may be partially responsible for the enhancement of cell motility and re-epithelialization in the presence of W379. The synergistic influence of the nanofiber aerogels with precision macrochannels and W379 peptide in promoting wound healing was illustrated in Figure 7. In the control group, only marginal cell infiltration and re-epithelialization took place on the wounds. In the aerogel-NC group, limited cell infiltration and re-epithelialization were noticed. In the aerogel-WC group, more cell infiltration/granulation tissue formation and partial re-epithelialization were observed. In the aerogel-WC+W379 group, more cell infiltration/granulation tissue formation and full re-epithelialization was completed.

3. Conclusions

In summary, we demonstrated the development of LL-37 mimetic W379 peptide incorporated PGLA/gelatin:PDO/gelatin nanofiber aerogels with precision macrochannels for healing diabetic wounds in mice. We also showed that the W379 peptide can enhance skin cell migration in an *in vitro* wound-healing assay. *In vivo* studies indicated patterned macrochannels in nanofiber aerogels can greatly enhance vascularized granulation tissue formation and the addition of W379 can promote not only vascularized granulation tissue formation but also re-epithelialization. The enhanced wound healing by W379 could be

due to the activation of the p38 MAPK signaling pathway. Together, the strategy presented in this work may be promising in the management of diabetic wounds and other chronic wounds.

4. Experimental Section

Materials:

The polydioxanon (PDO), and poly(glycolide-co-lactide) (PGLA 90:10) were purchased from BMG INC. Japan. Fisher Scientific (Waltham, MA, USA) supplied the GA (alcoholic solution). Sigma-Aldrich (St. Louis, MO, USA) provided Type A Gelatin from Porcine Skin, Pluronic-F-127, and Triton X-100. Gibco (Thermo Fisher Scientific Inc., Waltham, MA, USA) supplied the minimum necessary medium (MEM), fetal bovine serum (FBS), and penicillin-streptomycin. Oakwood chemicals (Estill, SC, USA) supplied the hexafluoroisopropanol (HFIP). Following our prior research, LL-37 and W379 peptides were produced.[31–35]

Fabrication of Nanofiber Mats by Electrospinning:

In this study, electrospinning was used to fabricate different nanofiber mats, including PGLA/gelatin (1:1) and (ii) PDO/gelatin (1:1), following our previously established protocols.[26] To prepare the spinning solutions, pre-estimated amounts of the polymers were dissolved in HFIP. The resulting spinning solutions contained 8 % of PGLA:gelatin (1:1) and 8 % of PDO:gelatin (1:1). A rotating mandrel was used to collect the aligned electrospun nanofibers. The following electrospinning parameters were used: DC voltage = 15 kV, flow rate = 0.4–0.6 mL/h, and the distance between the spinneret and the collector = 10–15 cm. For crosslinking of the electrospun nanofibers, GA vapor from a 25 % ethanolic solution was used overnight.

Fabrication of 3D-printed Sacrificial Template:

3D printed alginate meshes were fabricated following our previous method with some modifications.[26, 48, 49] The 3D printer Allevi 1 that uses the STL files of the digital models produced the alginate meshes with predesigned patterns, by directing depositing on a cryogenic substrate. After the meshes were printed, they were crosslinked with a cold $CaCl_2$ bath (2.5%) for 10 min and then stored in water until further use.

Fabrication of Aerogels with and without Precision Macrochannels:

All of the aerogels in this study, with and without patterned macrochannels, were created using a freeze-casting technique with minor modifications to our previously reported procedure.[26] Cryostat was used to segment the nanofiber mats of PGLA/gelatin and PDO/gelatin before freeze-drying. The short nanofiber segments obtained were stored at 4 °C for future use. To make nanofiber aerogels with a 1:1 ratio of PGLA/gelatin and PDO/gelatin short nanofiber segments, the segmented nanofibers were dispersed in water at a concentration of 25 mg/mL for 40 min in an ice bath using a homogenizer with a 20% amplitude and 10/20 s ON/OFF cycles. After 40 min of homogenization, a small amount of gelatin (5 percent of the fiber content) was added, and homogenization was continued for another 20 min under the same conditions. The homogeneous mixture was

then transferred to a copper ring mold that was attached to an aluminum plate. After immersing the sacrificial template in the mold, the mixture was rapidly frozen on a metal plate in a deep freezer. The mold was immediately transferred to a −80 °C refrigerator for 1 h. The frozen mold was immediately transferred to a freeze drier and lyophilized for 24 h. The resulting aerogels were then crosslinked with GA vapor for 12 h in a closed chamber containing 1 mL of 50% GA in ethanol. We then immersed the aerogels containing the 3D-printed meshes in a 50-mM EDTA solution for 4–6 h to remove the sacrificial template. After crosslinking with GA, we washed with Tris buffer to remove the excess of GA bounded in the aerogels. Other green crosslinkers like genipin and tannic acid could be used to replace GA in case any negative effects were observed. Prior to in vitro and in vivo applications, the nanofiber aerogels were sterilized with 70% ethanol.

Morphology and Structure Characterizations by Scanning Electron Microscopy:

Scanning electron microscopy (SEM) was used to examine the morphologies of aerogels with and without patterned microchannels (FEI Quanta 200, Hillsboro, OR, USA). After removing the template, the aerogels were frozen in water and sectioned horizontally and longitudinally with a cryostat, followed by freeze-drying to dry the aerogels. The freeze-dried aerogels were sputter-coated in the Ar atmosphere with an Au-Pd target at a peak current of 15 A for 5 min after being mounted onto a metallic stub with double-sided conductive carbon tape. Following that, the aerogels were imaged with an accelerating voltage of 15–25 kV.

Cell Culture:

The HaCat cells and HDFs from ATCC were cultured in MEM in the presence of 10% FBS and 1% penicillin-streptomycin a 10-cm culture dish and incubated at 37 °C under 5% CO_2. After reaching 80% confluence, cells were used for further studies such as cell viability and migration assays.

Cell Viability Assays:

The Cell Count Kit-8 (CCK-8, Dojindo Molecular Technologies, MD, USA) was used to quantitatively evaluate cell viability. HaCat and HDF cells were seeded in 96-well plates at a density of 5000 cells per well. After 30 min, LL37 and W379 peptides were added to the culture medium (DMEM with 10% FBS and 1% antibiotics) to form various concentrations ranging from 1μg/mL to 7 μg/mL and incubated for 24 h. After incubation, the CCK-8 solution (50 μL per well) was added to each well and the absorbance at 450 nm was determined using a microplate reader. Three replicate samples were tested at each time point.

In vitro Wound Healing Assay (Scratch Assay):

HaCaT and HDF cells were seeded to 24-well plates. After reaching 90% of confluency, the cell growth was arrested with 250 μL of 5 μg/mL of mitomycin C. After incubation of the plates for 2 h, the mitomycin C containing media was removed from the culture wells and cells were washed with PBS for 3 times. Then, artificial wounds were created by using 200 μL tips in both HaCat and HDF cell monolayers. The wound margins were photographed at t

= 0 h. Then, cells were treated with different concentrations (1 μg to 7 μg) of LL-37 peptide and W379 peptide for up to 24 h. The same fields of the wound margin were photographed at different time points like t = 12 h and 24 h by using Leica DMi1 microscope and LAS EZ software. The percentage of area that cells covered in the artificial wound region was calculated by using image J.

Western Blotting Analysis:

3×10^5 HaCat cells were plated in each well of a 6- well plate. After 24 h of plating, the cells were treated with either W379 or LL-37 peptides at a concentration of 3 μg/mL for varying time periods along with a control set which received no peptides. The cells were lysed with ice-cold lysis buffer containing RIPA buffer (pH 7.4) along with a combination of protease inhibitors, 20 μg/mL Leupeptin, 10 μg/mL Aprotinin, 1 mmol/L PMSF, and Halt protease. The total protein was collected and estimated using the Bradford reagent. SDS-PAGE was run, and the samples were transferred onto a PVDF membrane. Following this, the membrane was blocked with 5% w/v BSA in TBST for 30 min and probed with primary antibody (phosphor- p38 MAPK, total p38 MAPK, phosphor-STAT3, total STAT3, β-actin antibodies from cell signaling) overnight. The membrane was washed with 1×TBST and incubated with the secondary antibody conjugated with HRP for 1 h in 1×TBST at room temperature. The membrane was washed, and the protein bands were detected using super signal west Femto Maximum Sensitivity Substrate (Bio-rad). The protein bands were compared with the protein ladder and presented. Densitometry analysis of the bands was conducted using Image J. Band intensity of phosphorylated protein to total protein was calculated and the fold change represented as a graph with mean of three separate experiments and standard error of mean.

In vivo Study:

The TALLYHO type 2 diabetic mice (Male, 10–12 weeks, The Jackson Laboratory) were anesthetized for approximately 2 min with 4 % isoflurane in oxygen. Mice were placed on a heating pad to keep their body temperature stable. Each animal's back was shaved in a 44 cm^2 area, and the povidone-iodine solution was applied three times to the exposed skin. A skin punch was then used to create a circular wound (8 mm in diameter). The control wounds were left untreated after the wound model was established (n = 8). One group of wounds were treated with nanofiber aerogels without channels (Aerogel-NC) (n = 8). Another group of wounds were treated with nanofiber aerogels with channels (Aerogel-WC) (n = 8). The additional group of wounds were treated with W379 peptide (100 μg/Aerogel) added to the nanofiber aerogels (Aerogel-WC+W379) (n = 8) after the implantation. There were four mice in each group at each time point, with a total of eight wounds in each group at each time point. On days 7 and 14, after the aerogels were implanted, a digital camera was used to record the wounds of each mouse. The wound and surrounding tissues were then excised and fixed in 4% paraformaldehyde. IACUC (Protocol #19-069-07-FC) at the University of Nebraska Medical Center (UNMC) approved the animal study.

Histology:

Fixed samples were dehydrated in a graded ethanol series (70–100%), embedded in paraffin, and sectioned (5-μm thick). Standard procedures were followed to stain the samples with

hematoxylin and eosin (H & E) or Masson's trichrome. The area of cell infiltration was then quantified using Image J. The neovascularization was counted per cm^2 in both H & E and trichrome stained images, as well as immunohistochemical studies, after the paraffin-embedded samples were deparaffinized and rehydrated with xylene, followed by a series of ethanol washes. Antigen epitope unmasking was accomplished by boiling the tissues for 15 min in a citrate based (pH 6.0) antigen unmasking solution (Vector laboratories). Following that, the samples were allowed to cool to room temperature before being washed twice with distilled water and treated for 20 min with 3% hydrogen peroxide in methanol. The tissues were then washed with distilled water and incubated for 1 h at room temperature in blocking buffer (5 percent goat serum in Tris-buffered base containing tween 20 (TBST)). The tissues were incubated overnight at 4 °C with primary antibody (1:500 dilution of Pan cytokeratin from Abcam) diluted in blocking buffer. The tissue samples were washed in TBST three times for 5 min each before being incubated with biotinylated secondary antibody for 1 h. The samples were washed three times in TBST for 5 min each. The tissues were incubated with avidin-biotin complex for 30 min at room temperature according to the manufacturer's instructions and was developed using diaminobenzidine solution containing 0.3 percent H_2O_2 as a substrate for peroxidase (Dako). Hematoxylin was used to counterstain the tissues, which were then washed with tap water. The tissues were dehydrated in a series of ethanol washes to xylene before being mounted with Permount and covered with glass coverslips. The entire set of slides was then digitally scanned at UNMC's Tissue Science Facility to obtain images for visualization.

To quantify the cellular infiltration, the H & E-stained images were used to calculate the cellular infiltration in the implanted materials after the healing. We calculate the area of cell infiltration by using Image J software (n=3). The H & E-stained images (n=3) from different mice in each group were used to calculate the area of cell infiltration. The area of the implanted site (8 mm defect) was calculated, denoted as an area of the defect (Ad). We further calculated the area of cell infiltrated inside the aerogel based on migrated cells in the aerogel, denoted an area of cell infiltration (ACin). Then we calculated the percentage of cell infiltration by ACin/Ad*100 %.

We quantified neovascularization in each diabetic wound as follows. The trichrome-stained images were used to quantify the neovascularization or blood vessel sprouting in the implanted sites in the diabetic wounds by manually counting vessels with fine lumen walls in the erythrocytes present in the wall in each image (n=3). The reepithelization was measured by using Cytokeratin 6a immunostaining images. We measured the length of the newly formed keratinocyte layer on the top of the aerogel from each side (n=3). Reepithelialization ratio = measured total length/original defect length*100%.

Statistical Analysis:

All cell culture experiments and histology analysis were repeated three times (n=3), and the data presented are the mean ± standard deviation. The statistical analysis was carried out using the SPSS software version 2.0. One-way ANOVA with Tukey test was used to determine the statistical significance. Each data set was analyzed and significance was denoted as ns ≥ 0.05, *p < 0.05, **p < 0.01, ***p < 0.001, ****p < 0.0001. In addition,

the fold change of phosphorylated protein to total protein represented as a graph with mean of three separate experiments and standard error of mean. Statistical significance was calculated using two-way ANOVA in graphpad prism and depicted as *p<0.05, **p<0.01.

Supplementary Material

Refer to Web version on PubMed Central for supplementary material.

Acknowledgments

This work was partially supported by startup funds from the University of Nebraska Medical Center (UNMC), National Institute of General Medical Science (NIGMS) of the National Institutes of Health under Award Numbers R01GM138552 (J.X. and G. W.) and R01GM134036 (Y. S. Z.), Nebraska Research Initiative grant, and NE LB606.

References

[1]. Alejandro AE, Taghva S, Chapman C, Bowker JH, Orthopedics 2011, 34, e885. [PubMed: 22146206]

[2]. Singh N, Armstrong DG, Lipsky BA, JAMA 2005, 293, 217. [PubMed: 15644549]

[3]. Alavi A, Sibbald RG, Mayer D, Goodman L, Botros M, Armstrong DG, Woo K, Boeni T, Ayello EA, Kirsner RS, J. Am. Acad. Dermatol 2014, 70, 1.e1.

[4]. Rice JB, Desai U, Alice Kate G, Cummings BA, Diabetes Care 2014, 37, 651. [PubMed: 24186882]

[5]. Skrepnek GH, Mills JL Sr, Armstrong DG, PLoS One 2015, 10, e0134914. [PubMed: 26248037]

[6]. Hicks CW, Selvarajah S, Mathioudakis N, Sherman RE, Hines KF, Black JH, Abularrage CJ, Ann. Vasc. Surg 2016, 33, 149. [PubMed: 26907372]

[7]. Lin C, Liu J, Sun H, PLoS One 2020, 15, e0239236. [PubMed: 32936828]

[8]. Raghav A, Khan ZA, Labala RK, Ahmad J, Noor S, Mishra BK, Ther. Adv. Endocrinol. Metab 2018, 9, 29. [PubMed: 29344337]

[9]. Chen S, Li R, Li X, Xie J, Adv. Drug Del. Rev 2018, 132, 188.

[10]. Xue J, Xie J, Liu W, Xia Y, Acc. Chem. Res 2017, 50, 1976. [PubMed: 28777535]

[11]. Chen S, Liu B, Carlson MA, Gombart AF, Reilly DA, Xie J, Nanomedicine 2017, 12, 1335. [PubMed: 28520509]

[12]. Xue J, Wu T, Dai Y, Xia Y, Chem. Rev 2019, 119, 5298. [PubMed: 30916938]

[13]. Chen S, John JV, McCarthy A, Xie J, J. Mater. Chem. B 2020, 8, 3733. [PubMed: 32211735]

[14]. Rnjak-Kovacina J, Weiss AS, Tissue Eng. B 2011, 17, 365.

[15]. Jiang J, Carlson MA, Teusink MJ, Wang H, MacEwan MR, Xie J, ACS Biomater. Sci. Eng 2015, 1, 991. [PubMed: 33429530]

[16]. Jiang J, Li Z, Wang H, Wang Y, Carlson MA, Teusink MJ, MacEwan MR, Gu L, Xie J, Adv. Healthcare Mater 2016, 5, 2993.

[17]. Chen S, Carlson MA, Zhang YS, Hu Y, Xie J, Biomaterials 2018, 179, 46. [PubMed: 29980074]

[18]. Jiang J, Chen S, Wang H, Carlson MA, Gombart AF, Acta Biomater. 2018, 68, 237. [PubMed: 29269334]

[19]. Chen S, Wang H, McCarthy A, Yan Z, Kim HJ, Carlson MA, Xia Y, Xie J, Nano Lett. 2019, 19, 2059. [PubMed: 30788971]

[20]. Chen S, John JV, McCarthy A, Carlson MA, Li X, Xie J, Apply. Phys. Rev 2020, 7, 021406.

[21]. Chen S, McCarthy A, John JV, Su Y, Xie J, Adv. Mater 2020, 32, 2003754.

[22]. Wang L, Qiu Y, Guo Y, Si Y, Liu L, Cao J, Yu J, Li X, Zhang Q, Ding B, Nano Lett 2019, 19, 9112. [PubMed: 31765166]

[23]. Wang L, Qiu Y, Lv H, Si Y, Liu L, Zhang Q, Cao J, Yu J, Li X, Ding B, Adv. Funct. Mater 2019, 29, 1901407.

[24]. Weng L, Boda SK, Wang H, Teusink MJ, Shuler FD, Xie J, Adv. Healthcare Mater 2018, 7, e1701415.

[25]. Li R, Wang H, John JV, Song H, Teusink MJ, Xie J, Adv. Funct. Mater 2020, 30, 2005531. [PubMed: 34326714]

[26]. John JV, McCarthy A, Wang H, Luo Z, Li H, Wang Z, Cheng F, Zhang YS, Xie J, Adv. Healthcare Mater 2021, 10, 2100238.

[27]. Michelle Kahlenberg J, Kaplan MJ, J. Immunol 2013, 191, 4895. [PubMed: 24185823]

[28]. Duplantier AJ, van Hoek ML, Front. Immunol 2013, 4, 143. [PubMed: 23840194]

[29]. Ramos R, Silva JP, Rodrigues AC, Costa R, Guardao L, Schmitt F, Soares R, Vilanova M, Domingues L, Gama M, Peptides 2011, 32, 1469. [PubMed: 21693141]

[30]. Gronberg A, Mahlapuu M, Stahle M, Whately-Smith C, Rollman O, Wound Repair Regen. 2014, 22, 613. [PubMed: 25041740]

[31]. Li X, Li Y, Han H, Miller DW, Wang G, J. Am. Chem. Soc 2006, 128, 5776. [PubMed: 16637646]

[32]. Wang G, J. Biol. Chem 2008, 283, 32637. [PubMed: 18818205]

[33]. Mishra B, Narayana JL, Lushnikova T, Wang X, Wang G, Proc. Natl. Acad. Sci. USA 2019, 116, 13517. [PubMed: 31209048]

[34]. Narayana JL, Mishra B, Lushnikova T, Wu Q, Chhonker YS, Zhang Y, Zarena D, Salnikov E, Dang X, Wang F, Murphy C, Foster KW, Gorantla S, Bechinger B, Murry DJ, Wang G, Proc. Natl. Acad. Sci. USA 2020, 117, 19446. [PubMed: 32723829]

[35]. Su Y, Mainardi VL, Wang H, McCarthy A, Zhang YS, Chen S, John JV, Wong SL, Hollins RR, Wang G, Xie J, ACS Nano 2020, 14, 11775. [PubMed: 32840361]

[36]. Koczulla R, von Degenfeld G, Kupatt C, Krötz F, Zahler S, Gloe T, Issbrücker K, Unterberger P, Zaiou M, Lebherz C, Karl A, Raake P, Pfosser A, Boekstegers P, Welsch U, Hiemstra PS, Vogelmeier C, Gallo RL, Clauss M, Bals R. J Clin Invest. 2003, 111, 1665. [PubMed: 12782669]

[37]. Yin J, Yu FS Invest Ophthalmol Vis Sci. 2010, 51, 1891. [PubMed: 19797203]

[38]. Tokumaru S, Sayama K, Shirakata Y, Komatsuzawa H, Ouhara K, Hanakawa Y, Yahata Y, Dai X, Tohyama M, Nagai H, Yang L, Higashiyama S, Yoshimura A, Sugai M, Hashimoto K. J. Immunol 2005,175, 4662. [PubMed: 16177113]

[39]. Heilborn JD, Nilsson MF, Kratz G, Weber G, Sørensen O, Borregaard N, Ståhle-Bäckdahl M. J. Invest. Dermatol 2003, 120, 379. [PubMed: 12603850]

[40]. Pillai CKS, Sharma CP, J. Biomater. Appl 2010, 25, 291. [PubMed: 20971780]

[41]. MacEwan MR, MacEwan S, Kovacs TR, Batts J, Cureus 2017, 9, e1736. [PubMed: 29209583]

[42]. Schonauer C, Tessitore E, Barbagallo G, Albanese V, Moraci A, Eur. Spine J 2004, 13, S89. [PubMed: 15221572]

[43]. Woodruff M, Hutmacher D, Prog. Polym. Sci 2010, 35, 1217.

[44]. Shibata S, Tada Y, Asano Y, Hau CS, Kato T, Seki H, Yamauchi T, Kubota N, Kadowaki T, Sato S, J. Immunol 2012, 189, 3231. [PubMed: 22904306]

[45]. Sano S, Itami K, Tarutani M, Yamaguchi Y, Miura H, Yoshikawa K, Akira S, Takeda J, EMBO J. 1999, 18, 4657. [PubMed: 10469645]

[46]. Patel S, Srivastava S, Singh MR, Singh D, Biomed. Pharmacother 2019, 112, 108615. [PubMed: 30784919]

[47]. Dabiri G, Damstetter E, Philips T, Adv. Wound Care 2016, 5, 32.

[48]. Ravanbakhsh H, Luo Z, Zhang X, Maharjan S, Mirkarimi HS, Tang G, Chavez-Madero C, Mongeau L, Zhang YS, Matter 2022, 5, 573. [PubMed: 35695821]

[49]. Luo Z, Tang G, Ravanbakhsh H, Li W, Wang M, Kuang X, Garciamendez-Mijares CE, Lian L, Yi S, Liao J, Xie M, Guo J, Zhou Z, Zhang YS, Adv. Mater 2022, 34, 2270091.

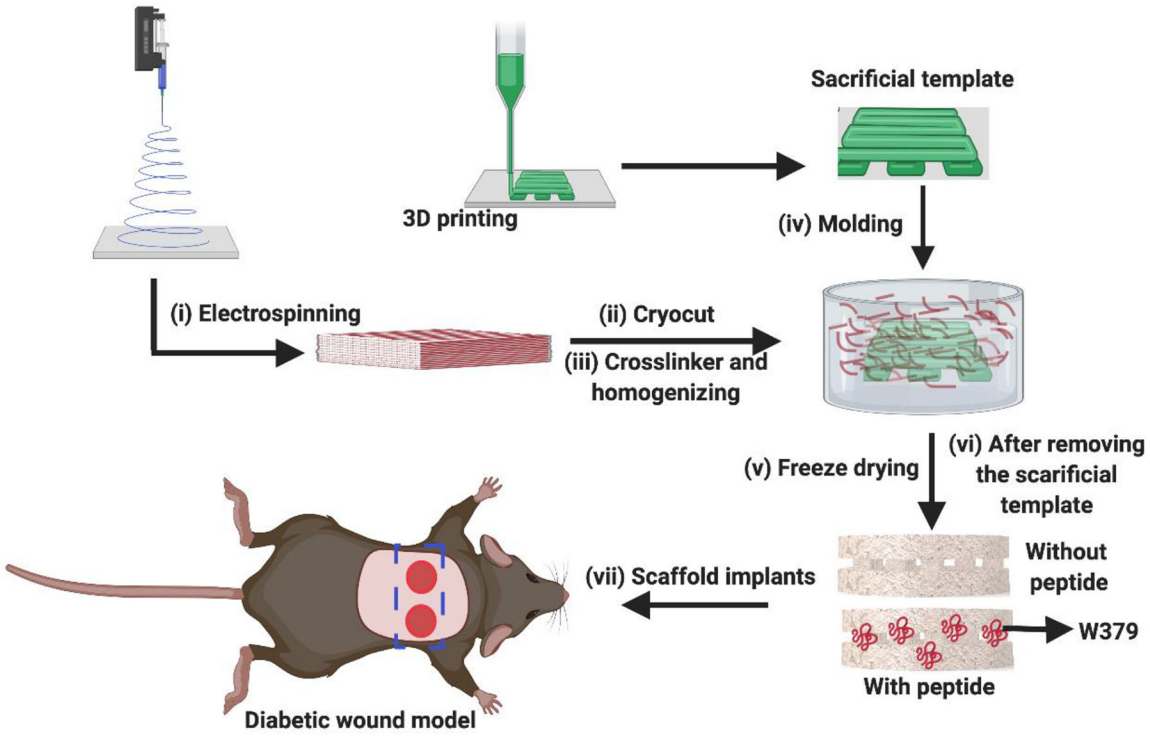

Figure 1. Schematic illustration of the fabrication of nanofiber aerogels with precision macrochannels incorporated with W379 peptide for healing diabetic wounds in mice.

i) Fabrication of PGLA (90:10)/gelatin (1:1) and PDO/gelatin (1:1) nanofiber mats via electrospinning, ii) Segmenting the nanofiber mats into short nanofibers through cryocutting, iii) Homogenizing the segmented short nanofibers with crosslinker gelatin in water, iv) Molding with and without predesigned 3D-printed meshes, v) Freeze-drying the short nanofiber solutions with and without sacrificial templates, vi) Crosslinking and removing the sacrificial templates, and vii) Impanting the nanofiber aerogels with and without incorporation of W379 peptide to the diabetic wounds in mice.

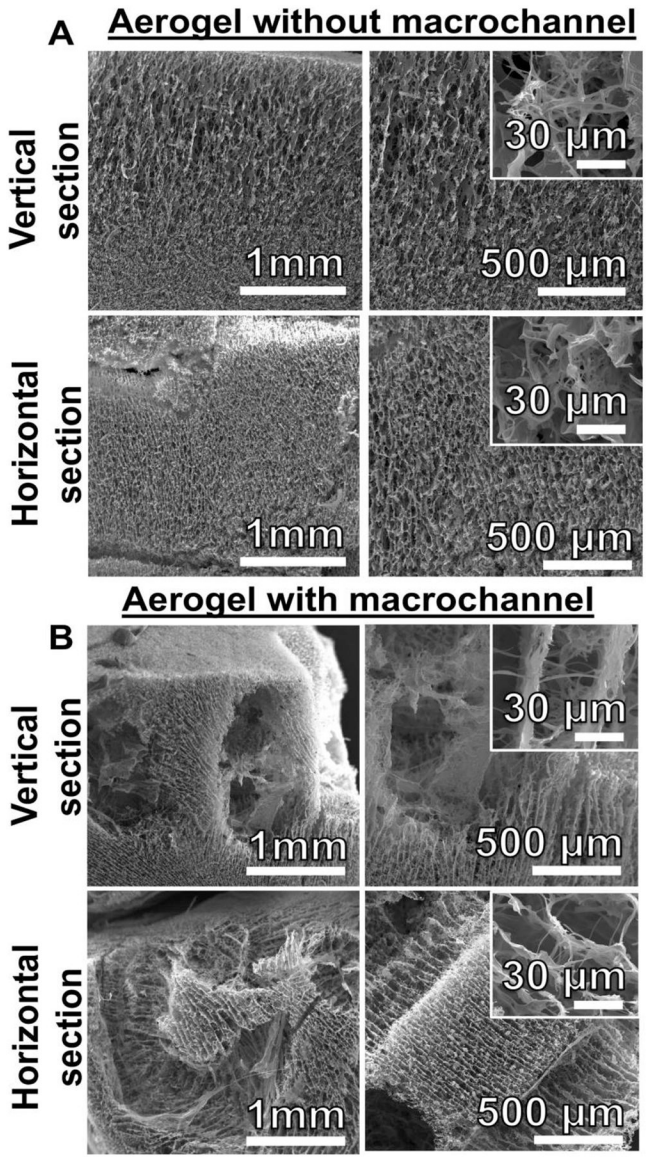

Figure 2. SEM images of nanofiber aerogels with and without precision macrochannels.

(A) The vertical and horizontal cross-sections of PDO/gelatin:PGLA/gelatin (1/1:1/1) short nanofiber composed aerogels without patterned macrochannel. (B) The vertical and horizontal cross-section of PDO/gelatin:PGLA/gelatin (1/1:1/1) short nanofiber composed aerogels with predesigned and patterned macrochannels.

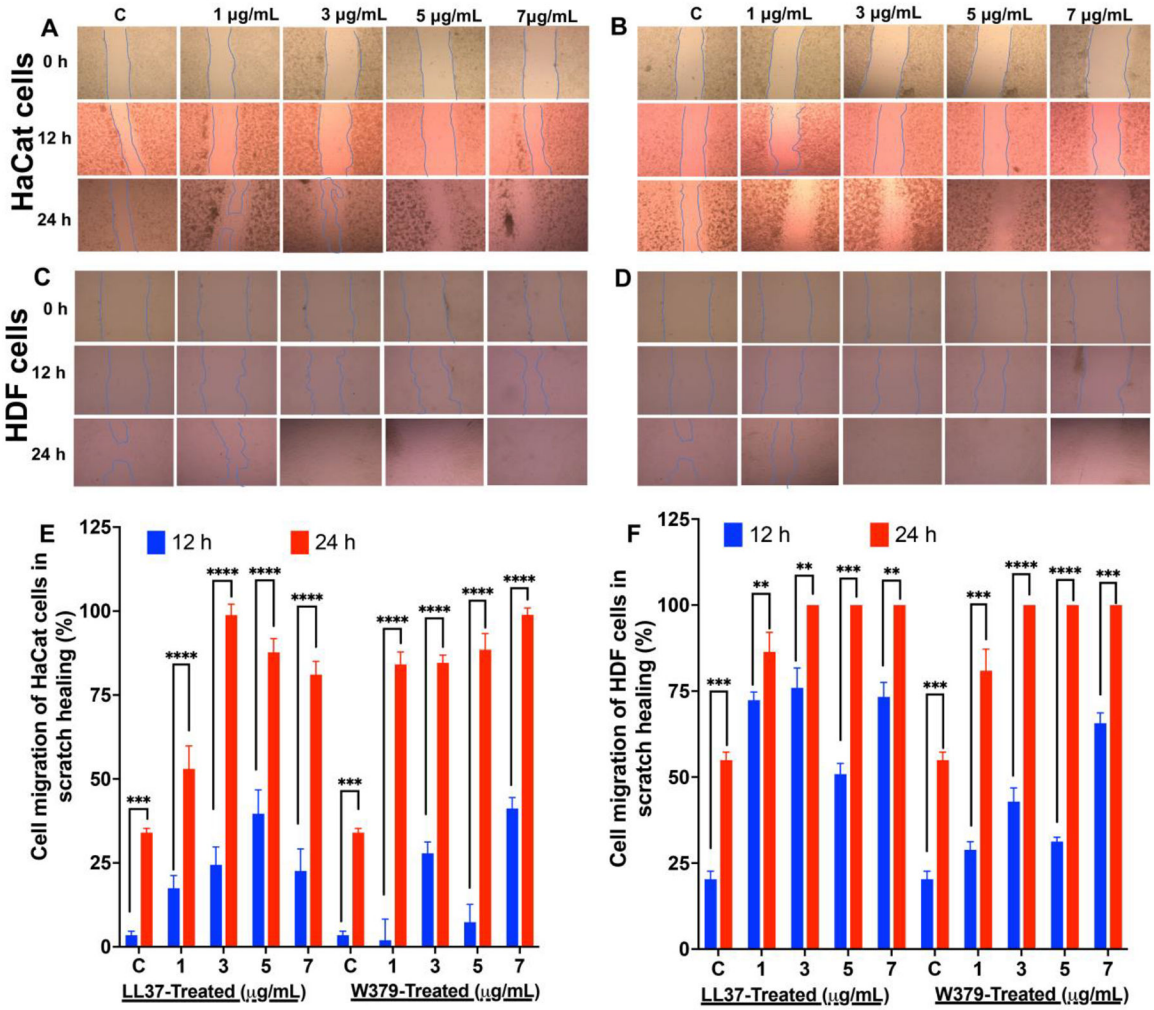

Figure 3. Scratch assay and cell migration analysis.

(A) Representative bright field images show the migration of HaCat cells in the scratch area after treated with different concentrations of W379 peptide. (B) Representative bright field images show the migration of HaCat cells in the scratch area after treated with different concentrations of LL-37 peptide. (C) Representative bright field images show the migration of HDF in the scratch area after treated with different concentrations of W379 peptide. (D) Representative bright field images show the migration of HDF in the scratch area after treated with different concentrations of LL37 peptide. (E) Wound closure expressed in scratch assay of HaCat cells treated with LL37 and W379 peptide at different concentrations ranging from 1 µg/mL to 7 µg/mL. (F) Wound closure expressed in scratch assay of HDF treated with LL37 and W379 peptide at different concentrations ranging from 1 µg/mL to 7 µg/mL. **p<0.01, ***p<0.001, ****p<0.0001.

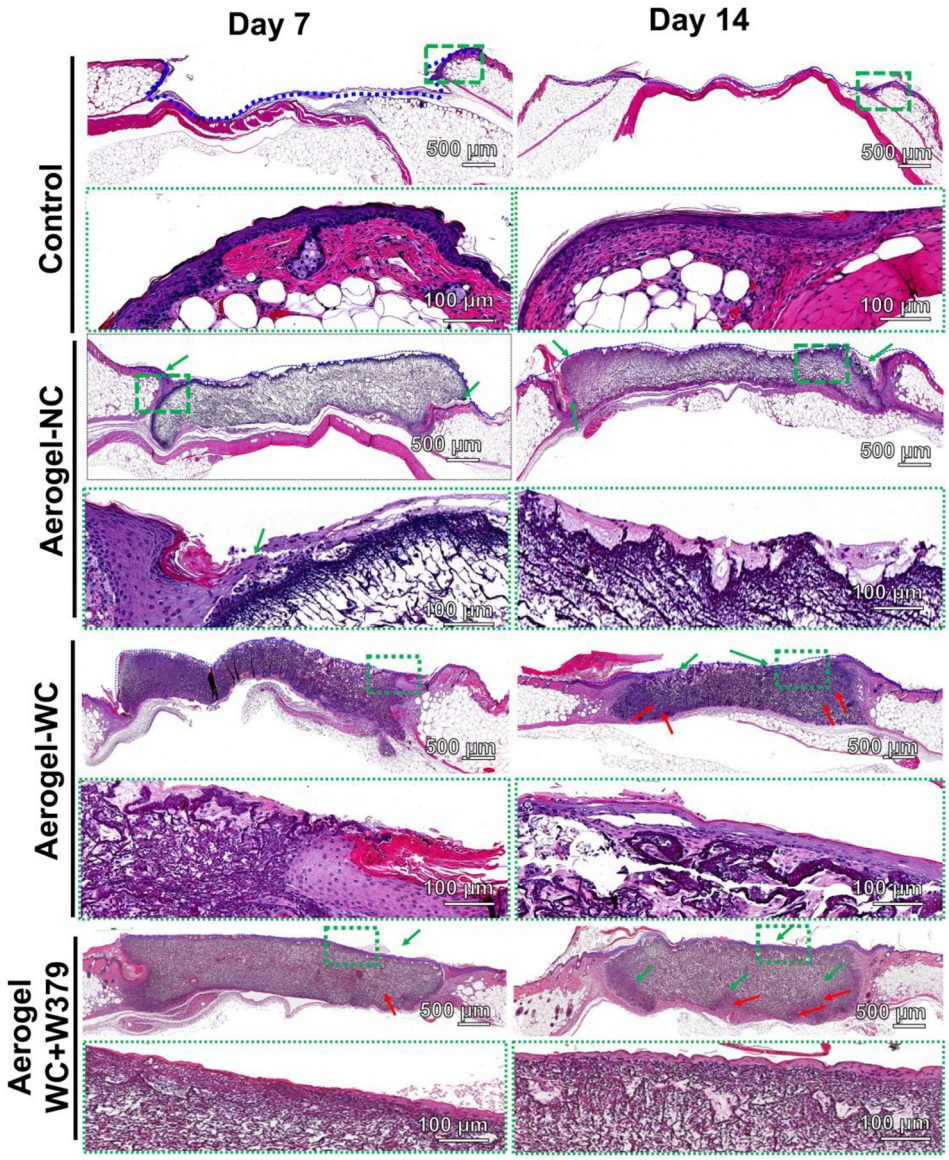

Figure 4. H&E staining images of wounds and surrrounding tissues isolated from type 2 diabetic mice after different treatments for 7 and 14 days.

H&E staining images of wounds and their surround tissues without treatment (control) and with treatment of Aerogel-NC, Aerogel-WC, and Aerogel-WC+W379 groups. Control: without treatment, Aerogel-NC: aerogels without macrochannels, Aerogel-WC: aerogels with precision macrochannels, Aerogel-WC+W379: W379 peptide incorporated aerogels with precision macrochannels.

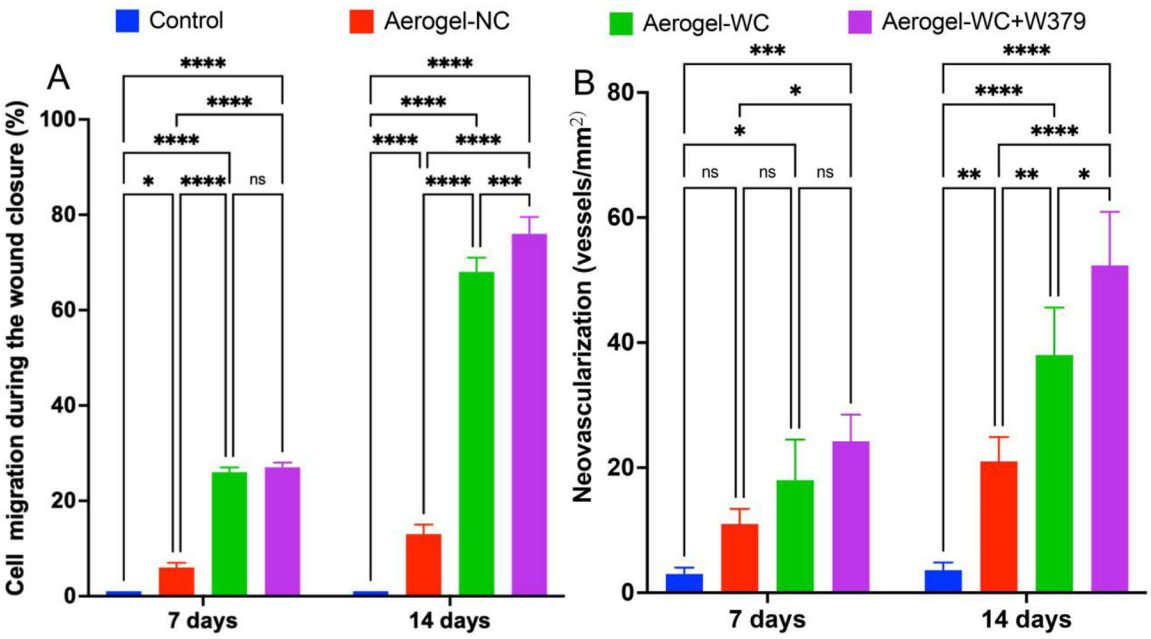

Figure 5. Cell infiltration and neovascularization in the type 2 diabetic mice wounds after different treatments for 7 and 14 days.

(A) Percentages of cell-infiltrated areas in wounds without treament (Control) and with treatment of Aerogel-NC, Aerogel-WC, and Aerogel-WC+W379 groups. (B) New blood vessel formation in the wounds without treament (Control) and with treatment of Aerogel-NC, Aerogel-WC, and Aerogel-WC+W379 groups. Control: without treatment, Aerogel-NC: aerogels without macrochannels, Aerogel-WC: aerogels with precision macrochannels, Aerogel-WC+W379: W379 peptide-incorporated aerogels with precision macrochannels. *p<0.05, **p<0.01, ***p<0.001, ****p<0.0001

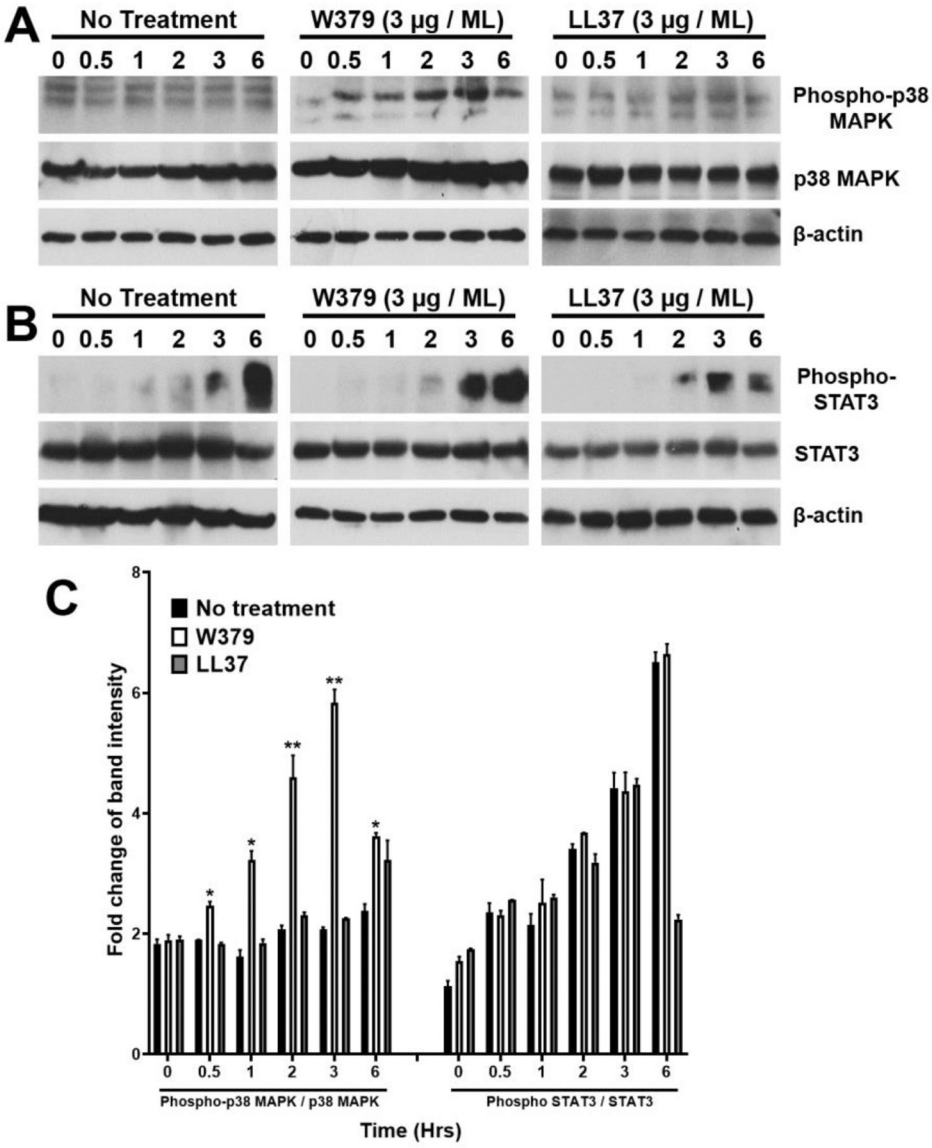

Figure 6. W379 peptide may promote keratinocyte migration via the p38 MAPK signaling pathway.

Total protein from HaCat cells treated with either W379 or LL-37 peptide (3 µg/mL) was analyzed for the phosphorylation status of p38 MAPK and STAT3 at varying time points. Non treated cells collected at respective time points served as control (No treatment). (A) Western blot depicting phospho-p38 MAPK and total p38 MAPK expression in control, W379 and LL-37 peptide treated cells. (B) Protein analysis of STAT3 phosphorylation status in control, W379 and LL37 peptide treated cells. (C) Quantitation of the densitometric analysis of all replicates corresponding to (A) and (B) conducted using Image J. Band intensity of phosphorylated protein to total protein was calculated and the fold change represented as a graph with statistical significance depicted as *$p<0.05$, **$p<0.01$.

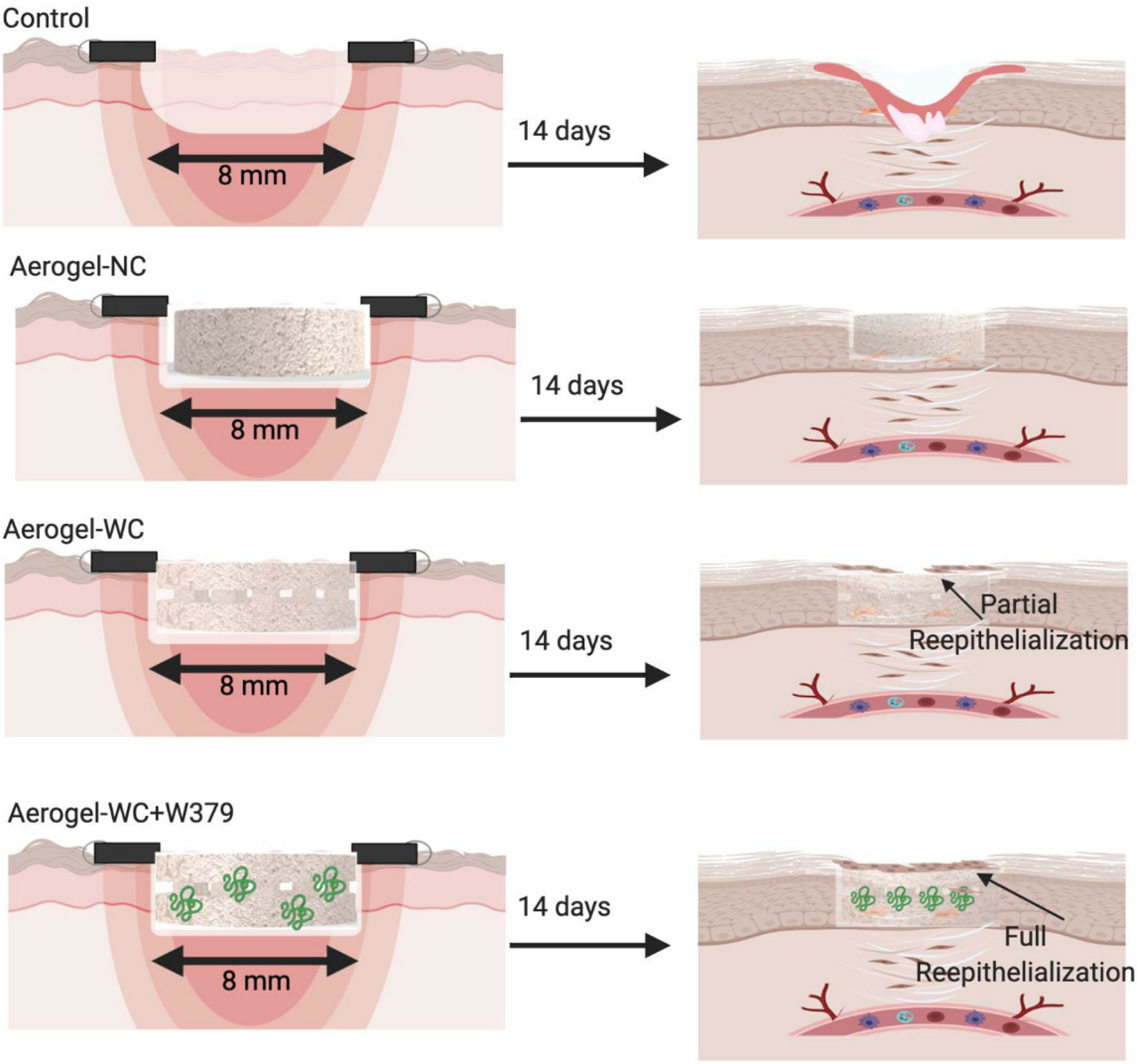

Figure 7. Schematic illustrating the potential mechanism of wound healing after different treatments.

Control: without treatment, Aerogel-NC: aerogels without macrochannels, Aerogel-WC: aerogels with predesigned and patterned macrochannels, Aerogel-WC+W379: W379 peptide-incorporated aerogels with predesigned and patterned macrochannels.